Virology 275, 306–317 (2000)
doi:10.1006/viro.2000.0507, available online at http://www.idealibrary.com on IDEAL®

Varicella-Zoster Virus gE Escape Mutant VZV-MSP Exhibits an Accelerated Cell-to-Cell Spread Phenotype in both Infected Cell Cultures and SCID-hu Mice

Richard A. Santos,* Christopher C. Hatfield,* Nancy L. Cole,† Jorge A. Padilla,* Jennifer F. Moffat,‡ Ann M. Arvin,‡ William T. Ruyechan,§ John Hay,§ and Charles Grose*,[1]

*Department of Microbiology, University of Iowa, Iowa City, Iowa 52242; †Indiana University School of Medicine, SBCME, Notre Dame, Indiana 46556; ‡Department of Pediatrics, Stanford University School of Medicine, Stanford, California 94305; and §Department of Microbiology, State University of New York at Buffalo, Buffalo, New York 14214

Received April 10, 2000; returned to author for revision May 10, 2000; accepted July 3, 2000

Varicella-zoster virus is considered to have one of the most stable genomes of all human herpesviruses. In 1998, we reported the unanticipated discovery of a wild-type virus that had lost an immunodominant B-cell epitope on the gE ectodomain (VZV-MSP); the gE escape mutant virus exhibited an unusual pattern of egress. Further studies have now documented a markedly enhanced cell-to-cell spread by the mutant virus in cell culture. This property was investigated by laser scanning confocal microscopy combined with a software program that allows the measurement of pixel intensity of the fluorescent signal. For this new application of imaging technology, the VZV immediate early protein 62 (IE 62) was selected as the fluoresceinated marker. By 48 h postinfection, the number of IE 62-positive pixels in the VZV-MSP-infected culture was nearly fourfold greater than the number of pixels in a culture infected with a low-passage laboratory strain. Titrations by infectious center assays supported the above image analysis data. Confirmatory studies in the SCID-hu mouse documented that VZV-MSP spread more rapidly than other VZV strains in human fetal skin implants. Generally, the cytopathology and vesicle formation produced by other strains at 21 days postinfection were demonstrable with VZV-MSP at 14 days. To assess whether additional genes were contributing to the unusual VZV-MSP phenotype, ~20 kb of the VZV-MSP genome was sequenced, including ORFs 31 (gB), 37 (gH), 47, 60 (gL), 61, 62 (IE 62), 66, 67 (gI), and 68 (gE). Except for a few polymorphisms, as well as the previously discovered mutation within gE, the nucleotide sequences within most open reading frames were identical to the prototype VZV-Dumas strain. In short, VZV-MSP represents a novel variant virus with a distinguishable phenotype demonstrable in both infected cell cultures and SCID-hu mice.

INTRODUCTION

Based on their extensive analyses of herpesviral molecular evolutionary history, McGeoch and Davison (1999) estimate that herpesvirus DNA sequences mutate 10–100 times faster than the equivalent classes of sequences on the host genome. For glycoprotein gB, a highly conserved open reading frame (ORF) among all herpesviruses, they calculate that nonsynonymous substitutions have occurred at a rate of 2.7×10^{-8} substitutions per site per year and synonymous substitutions at 10^{-7} substitutions per site per year (McGeoch and Davison, 1999). McGeoch and Davison (1999) also provide convincing arguments in favor of the concept of cospeciation; in other words, herpesvirus lineages arise by way of coevolution with their specific host. In the case of VZV, the progenitor virus most likely arose 60–70 million years before the present (McGeoch and Cook, 1994; McGeoch *et al.,* 1995).

Of all the human herpesviruses, VZV may undergo the fewest replication cycles during the lifetime of the infected host. Based on a probable schema of pathogenesis, the virus actively replicates for a period of 10–14 days after infection of the human host (Arvin, 1996; Grose, 1999). During a bout of chickenpox, therefore, VZV has at most 20 replication cycles. Based on our current understanding of VZV latency and reactivation, no further replication occurs unless the individual develops herpes zoster in late adulthood. Because of the above scenario, the genetic stability of the VZV genome has been presumed.

VZV contains the smallest genome of the human herpesviruses, encoding 69 ORFs within the complete VZV-Dumas sequence (Davison and Scott, 1983). Of these ORFs, at least 7 code for glycoproteins (Cohen and Straus, 1996; Grose, 1990; Mo *et al.,* 1999). VZV gE, the product of ORF 68, is the most abundantly produced viral glycoprotein during infection. Unlike other alphaherpesviral homologs, the VZV gE protein is a major antigenic determinant, inducing both cytolytic and humoral responses (Arvin *et al.,* 1986; Bergen *et al.,* 1991; Ito *et al.,* 1985). VZV gE, in complex with glycoprotein I (gI), acts as a human Fc receptor on the surface of infected cells

[1] To whom correspondence and reprint requests should be addressed at University Hospitals/2501 JCP, 200 Hawkins Drive, Iowa City, IA 52242. Fax: 319-356-4855. E-mail: charles-grose@uiowa.edu.

0042-6822/00 $35.00

(Litwin *et al.,* 1990, 1992). The cytoplasmic tails of both gE and gI contain endocytosis motifs, allowing internalization and recycling of the complex to and from the cell membrane (Olson *et al.,* 1997; Olson and Grose, 1997). The gE and gI cytoplasmic tails also are modified by both serine/threonine and tyrosine phosphorylation motifs (Olson *et al.,* 1997; Yao *et al.,* 1993; Ye *et al.,* 1999). The fact that gE cannot be deleted suggests that it is essential (Cohen and Seidel, 1993; Mallory *et al.,* 1997). Because of its important functions, the recent discovery of a VZV gE escape mutant (VZV-MSP) was completely unexpected; based on the prototypic VZV-Dumas sequence, the mutant gE protein contains a D150N substitution (Santos *et al.,* 1998). The current report provides a more complete characterization of the altered biological properties and genetic composition of this contemporary variant in VZV evolution. For the first time, we have discovered a VZV variant virus which has a cell-to-cell spread phenotype clearly distinguishable from that of previously characterized VZV strains.

RESULTS

Cell-to-cell spread phenotype of VZV-MSP

During our initial assessment of VZV-MSP, we observed that the egress of VZV-MSP particles in cell culture differed from that of other typical VZV laboratory strains, such as VZV-32 and VZV-Oka (Santos *et al.,* 1998). Like other VZV strains, however, infectious virus was not released into the culture medium. The fact that greater numbers of VZV-MSP particles were present on the surface suggested that cell-to-cell spread may be increased. Cell-to-cell spread has been assessed in both HSV-1 and PRV through measurement of plaque size in permissive cells or the number of cells infected within a typical plaque (Dingwell *et al.,* 1994; Tirabassi *et al.,* 1997; Tirabassi and Enquist, 1999). Neither technique is easily applicable in the VZV system given the formation of irregularly shaped syncytia by VZV in cell culture and the absence of cell-free virus in tissue culture. Therefore, we developed a technique to assess cell-to-cell spread through confocal microscopic examination.

We compared the spread of low-passage VZV-MSP to that of the low-passage laboratory strain VZV-32. Human melanoma cells were inoculated with either VZV-32 or VZV-MSP at a 1:8 ratio of infected:uninfected cells. At increasing intervals postinfection, the infected monolayers were probed with an antibody against the VZV immediate early protein 62 (IE 62). The number of cells expressing IE 62 and the intracellular localization of the protein were determined. This assay was based on the observation by Kinchington and Turse (1998) that VZV IE 62 is present in the nuclei of infected cells during early stages of infection, but then appears in the cytoplasm during later stages.

The confocal micrographs in Figs. 1A and 1B compare VZV-32 and VZV-MSP at 4 h postinfection. This time point represents the number of infected cells originally overlaid onto each monolayer. Both panels contained similar levels of IE 62-positive cells. Figures 1C and 1D compare VZV-32 and VZV-MSP at 24 h postinfection. The difference in extent of spread between VZV-MSP and VZV-32 was apparent. Figures 1E and 1F represent a typical focus of infection present in each monolayer when viewed at a higher magnification. For VZV-32 in Fig. 1E, 6–8 cells with advanced infection were present in each focus; IE 62 was present in both nucleus and cytoplasm. A few scattered cells adjacent to the infectious focus contained nuclei with IE 62 concentrated near the membrane; these cells represented a recent transfer of infectivity from the central focus. When the VZV-MSP culture was examined (Fig. 1F), large syncytia had already formed at 24 h postinfection. A typical syncytium contained 20–30 nuclei, an infectious focus three- to fourfold larger than that seen with VZV-32. This experiment was repeated four times with equivalent results.

Quantitative analysis of confocal images of VZV IE 62

To quantify the difference in cell-to-cell spread, multiple confocal images were analyzed with the image analysis programs called Brainvox tal_support programs (Frank *et al.,* 1997). Each confocal image is made up of 512 × 512 pixels, for a total of 262,144 pixels. We analyzed the green fluorescence channel representing the presence of VZV IE 62 within each confocal image. The image analysis program initially assigns a relative signal intensity within each pixel of the confocal image. Then, a threshold of signal intensity is calculated to remove background signals. This analysis facilitated quantitation of all pixels within each confocal image that contained IE 62. Thus, confocal microscopy of IE 62 coupled with image analysis facilitated a comparison of the extent of viral spread between two different VZV strains.

The results for this analysis are shown in Fig. 2. Note that there was no major difference between the extent of IE 62 spread for VZV-32 and VZV-MSP at 4, 8, and 12 h postinfection. The results at both 4 and 8 h, in particular, demonstrated that each monolayer was infected with a similar inoculum of infected cells. Also, the lack of a difference between the three time points (4–12 h) confirmed that the replication cycle for both VZV strains was greater than 12 h, in agreement with previous studies (Yamanishi *et al.,* 1980). However, at 24 h postinfection, there was a noticeable difference between the spread of VZV-MSP and VZV-32. The extent of VZV-MSP spread was at least twofold greater than that of VZV-32. At 48 h postinfection, this difference increased further, as the VZV-MSP spread was fourfold greater than that of VZV-32. Thus, image analysis provided a new method by which to measure differences in cell-to-cell spread be-

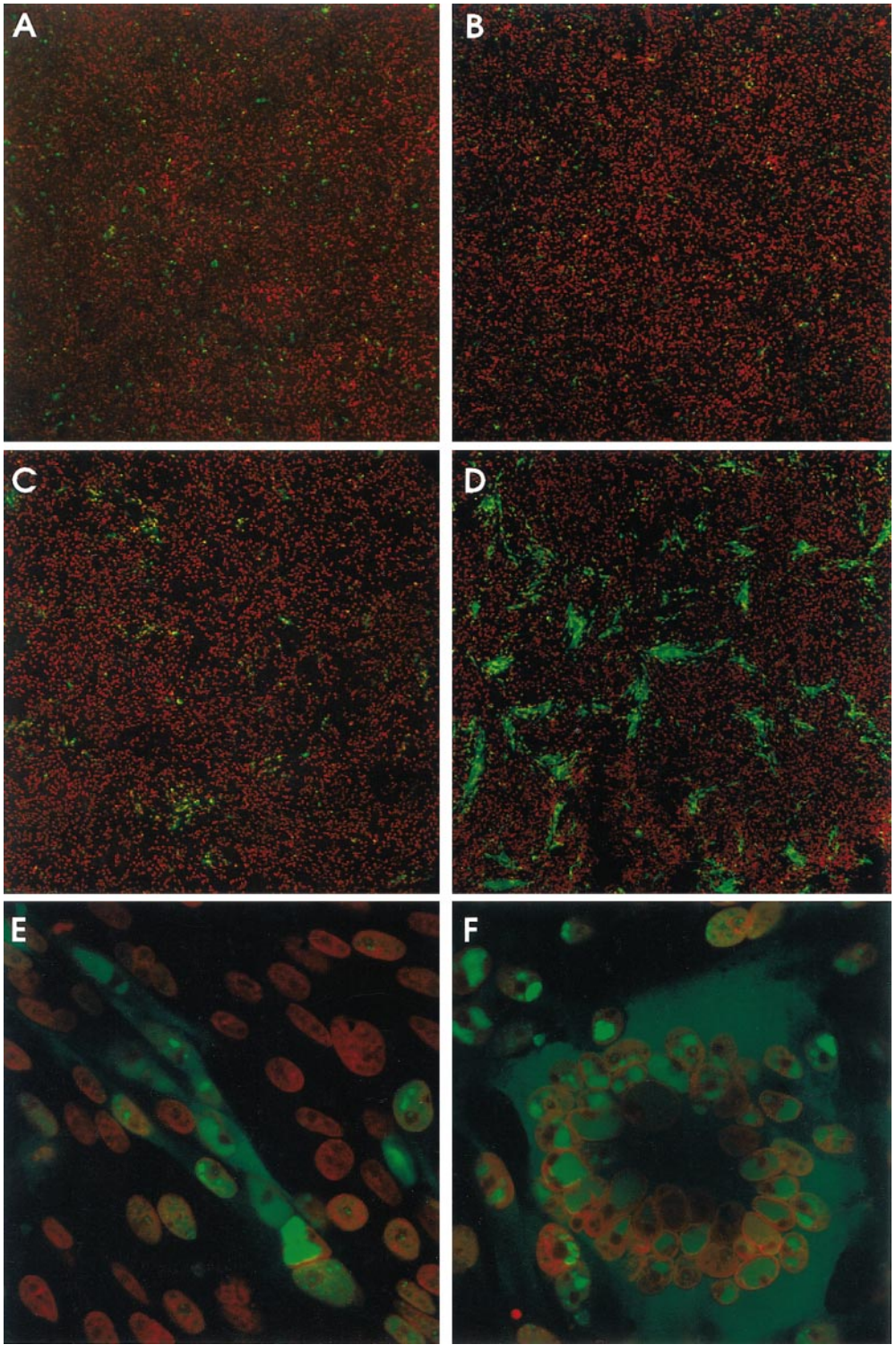

FIG. 1. Confocal microscopic imaging of VZV cell-to-cell spread. MeWo cell monolayers were infected with either VZV-32 (A, C, and E) or VZV-MSP (B, D, and F) and examined by laser scanning confocal microscopy. The fluoresceinated VZV IE 62 regulatory protein appears green while nuclei stained with TOTO-3 appear red. Infected monolayers were examined at 4 (A, B) and 24 h (C–F) postinfection. Original magnification: ×4 (A–D) and ×20 (E, F).

tween VZV strains. Again, this methodology is particularly suited for VZV because cell-free virus is not released spontaneously from infected cell cultures; even after sonic disruption of infected monolayers, most viral particles remain attached to remnants of outer cellular membranes (Grose and Brunell, 1978; Weller, 1953).

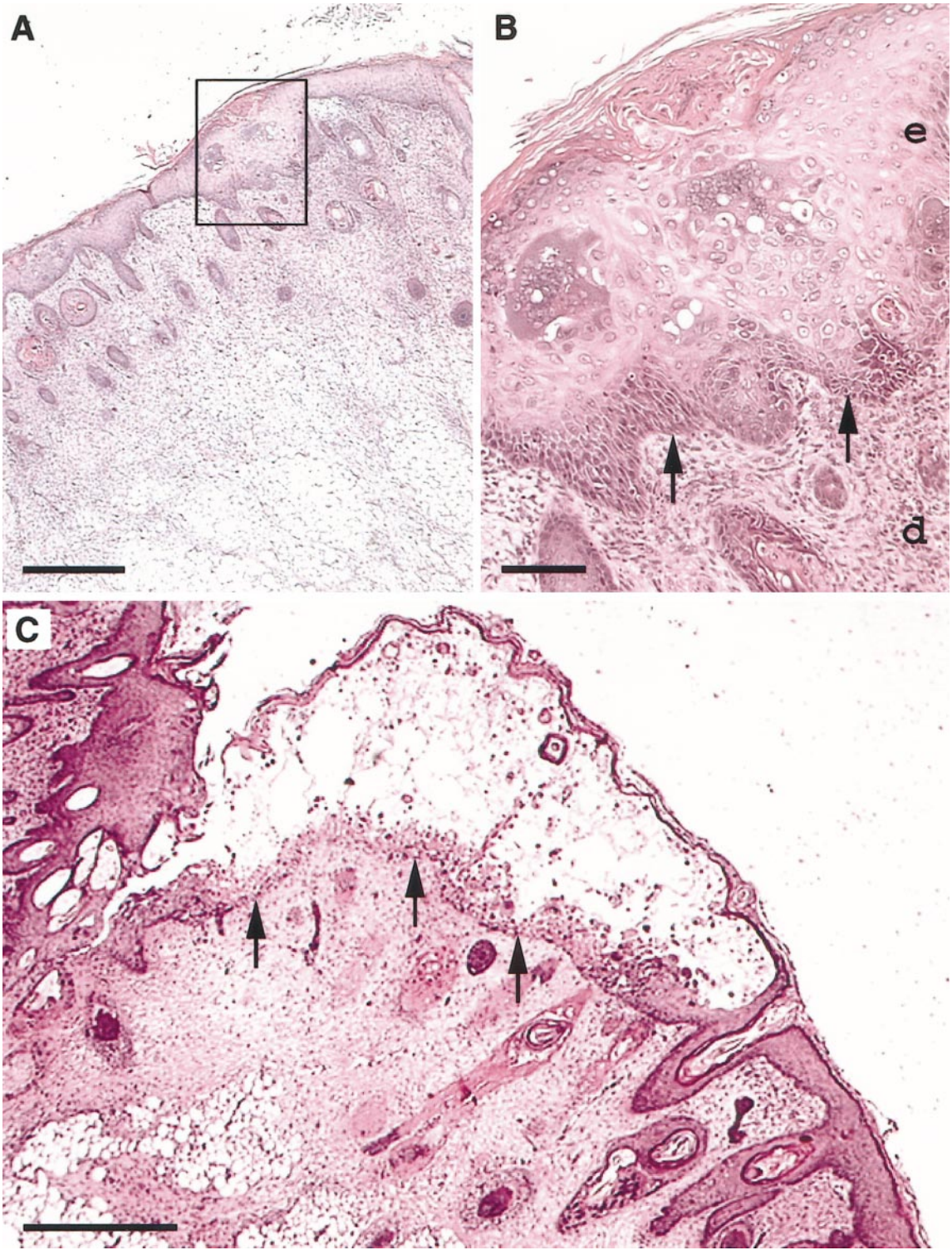

FIG. 4. Vesicle formation in the VZV-infected SCID-hu mouse model. Skin implants within the SCID-hu mice were harvested on days 7 and 14 postinfection with VZV-MSP; histological analyses were performed as described under Materials and Methods. (A) At day 7, early signs of infection were visible as small foci in the epidermis. (B) Enlarged view of boxed area in A. The infectious foci were visible in the epidermis (e). The basal lamina was intact (arrows) and the dermis was uninvolved (d). (C) By day 14, a representative vesicular lesion formed in the epidermis had greatly enlarged. The basal lamina was disrupted (arrows) and the virus had spread into the dermis. Magnification bars = 0.5 mm (A, C), 0.05 mm (B).

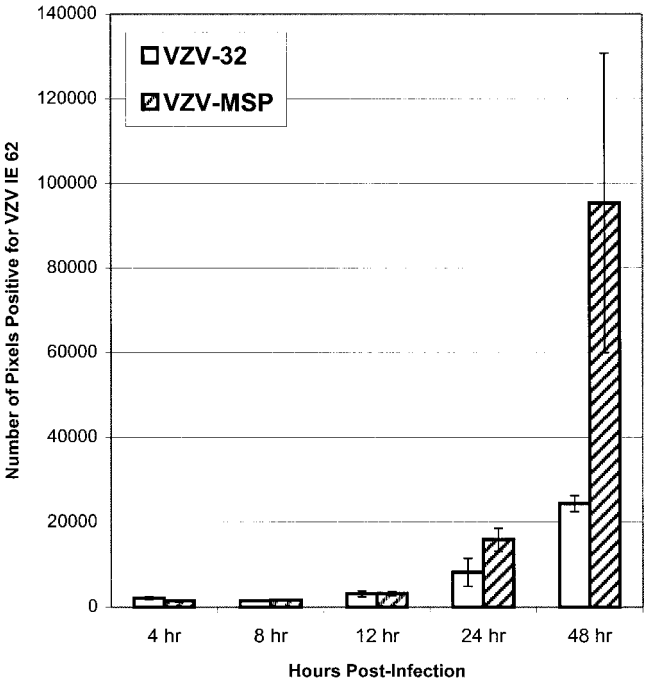

FIG. 2. Quantitative analysis of VZV IE 62 by confocal microscopy. VZV-MSP- or VZV-32-infected monolayers were examined by confocal microscopy at increasing times postinfection at ×4 original magnification. The total number of pixels positive for VZV IE 62 within each image was quantitated with the Brainvox tal_support programs (University of Iowa). The graph summarizes the results from four separate images. Error bars: ±1 SD.

VZV infectious center assays

Because the results in the previous experiments represented a new application of confocal microscopy, we turned to a traditional method to confirm the differences in VZV cell-to-cell spread, namely, infectious center assays (Cole and Kingsley, 1992; Grose and Brunell, 1978). For these titrations, the initial virus inocula were replicate samples of VZV-infected cells frozen and stored in liquid nitrogen. After being frozen, 1 aliquot was thawed and titrated from each lot. The inoculum for each 35-mm tissue culture dish was 500 infectious centers. Two dishes were harvested and assayed at each of the following time points: immediately after inoculation (0 h) and 24 and 48 h postinoculation (Fig. 3). When comparing the average fold increase of VZV-MSP infectious centers to VZV-32 infectious centers, the spread of VZV-MSP was consistently greater than the spread of VZV-32 over both the first 24-h period (24 h p.i.) and the second 24-h period (48 h p.i.). Otherwise stated, at 48 h postinfection, the cytopathic effect of VZV-MSP was complete, while numerous infectious center titrations with VZV-32 demonstrated that a 60- to 72-h interval was required for similar spread (Grose and Brunell, 1978). Furthermore, the rapidity of VZV-32 spread was not altered over the initial 20 passages. (VZV-Oka and VZV-Ellen titrations exhibit a time course similar to that of VZV-32; C. Grose, unpublished observations.) Therefore, results from both quantitative confocal microscopic image analyses and infectious center assays documented that the spread of VZV-MSP was three- to fourfold greater than the spread of VZV-32.

Growth of VZV-MSP in the SCID-hu mouse

The SCID-hu mouse has provided the first reproducible animal model of VZV pathogenesis. Published studies have documented the pathology of viral infection in human thymus/liver and skin implants after inoculation with parental and vaccine Oka strains as well as low-passage wild-type virus (Moffat *et al.,* 1995, 1998a). To assess whether VZV-MSP showed enhanced pathology in the SCID-hu mouse model, skin implants infected with VZV-MSP were harvested at 7, 14, and 21 days after infection. At 7 days postinfection, numerous foci of infection were visible in the epidermis of the human skin implant (Figs. 4A and 4B). By 14 days the foci coalesced into large necrotic lesions with histopathology typical of varicella vesicles (Fig. 4C). These vesicles were characterized by epidermal hyperplasia, balloon cells, and the separation of the keratin roof from the epidermis. After 21 days, the infection had spread into the dermis and destroyed the entire implant (Fig. 5A). Samples of the implants also were examined by previously described elec-

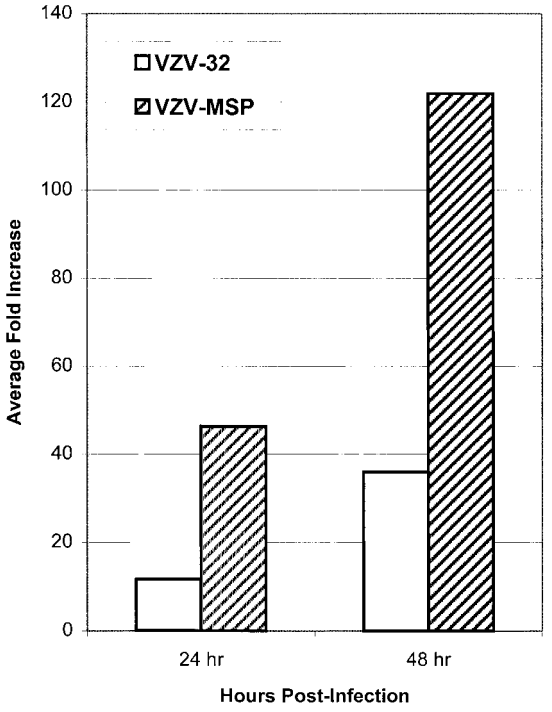

FIG. 3. Infectious center assays of VZV-MSP and VZV-32. Infectious center assays were carried out by previously described methods (Cole and Kingsley, 1992; Grose and Brunell, 1978). The numbers of infectious centers present at 24 and 48 h postinfection were determined for VZV-MSP and VZV-32. The average fold increase of infectious centers at each interval was tabulated.

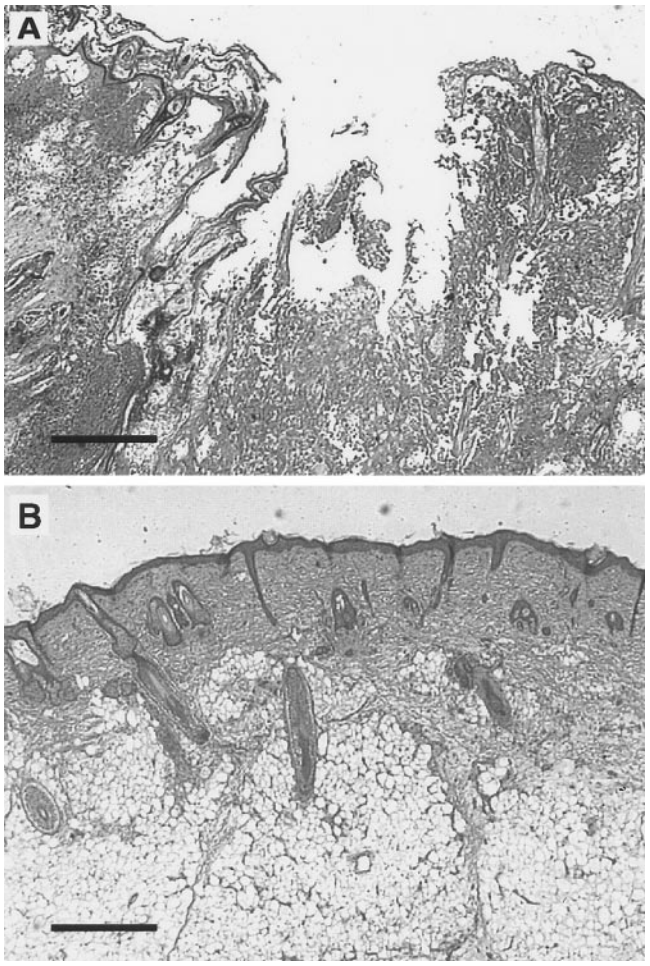

FIG. 5. Histological analysis of VZV-MSP infected skin implants at day 21. (A) VZV-MSP replication extended from the epidermis throughout the dermis and involved the entire implant, causing loss of normal skin architecture. Compare with Fig. 4. (B) Normal features of the epidermis and dermis were observed in the mock-infected control. Magnification bar = 0.5 mm.

tron microscopy methods; the virion formation closely resembled that shown in Fig. 2 of the report by Moffat *et al.* (1998a). Mock-infected skin implants showed normal skin structure consisting of a thin layer of keratinocytes above the dermis and hair follicles (Fig. 5B).

Prior published studies had not shown such a rapid progression of pathology in the SCID-hu mouse infected with VZV (Moffat *et al.,* 1995, 1998a). To further assess this aspect of VZV infection in the animal model, another experiment was performed with a clinical isolate passaged even fewer times than VZV-32; in addition, the low-passage parent VZV-Oka strain was included. Again, the skin samples were collected and examined at days 7, 14, and 21 postinoculation. When all the specimens were reviewed, the histopathology of the clinical isolate and parental VZV-Oka at 21 days postinoculation were similar, and for both strains the histopathology was approaching that caused by VZV-MSP at 14 days postinoculation (Fig. 6). Even at 21 days, however, the former two viral strains never caused the total destruction seen after VZV-MSP infection (Fig. 5A). In short, the progression of VZV-MSP through the skin implant was noticeably more extensive than that seen with other viral strains tested in the SCID-hu animal model (Figs. 4, 5, and 6).

Genetic analysis of other major glycoproteins of VZV-MSP

After documenting the enhanced cell-to-cell spread of VZV-MSP, we questioned whether mutations were present in ORFs other than gE that may be contributing to this phenotype. Specifically, we analyzed ORFs 31, 37, 60, and 67 coding for VZV gB, gH, gL, and gI, respectively. The ORFs were amplified from the VZV-MSP viral genome and sequenced and then compared to the published VZV-Dumas sequence (Davison and Scott, 1986). Of interest, neither the gI nor the gL gene contained any nucleotide differences when compared to the nucleotide

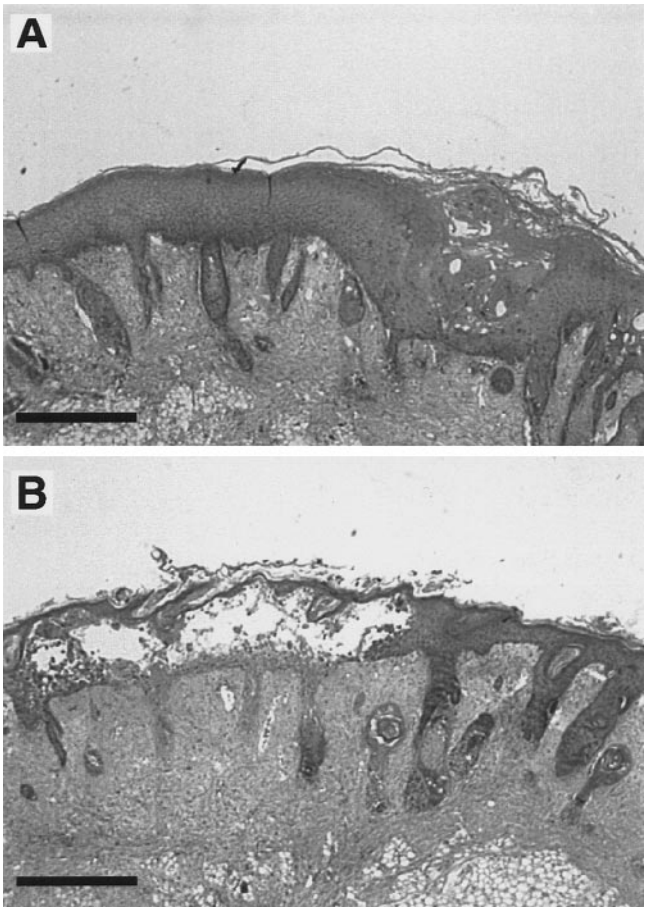

FIG. 6. Histological analysis of skin implants infected with parental VZV-Oka strain at day 21. These images highlight the range of cytopathology induced by parental VZV-Oka at day 21 p.i. (A) Small focus of infection in the epidermis of the skin implant with no evidence of penetration of the basal lamina. (B) Vesicle formation with penetration of the basal lamina and further infectious spread into the dermis. Compare with Fig. 5. Histopathology for clinical VZV isolate was similar (data not shown). Magnification bar = 0.5 mm.

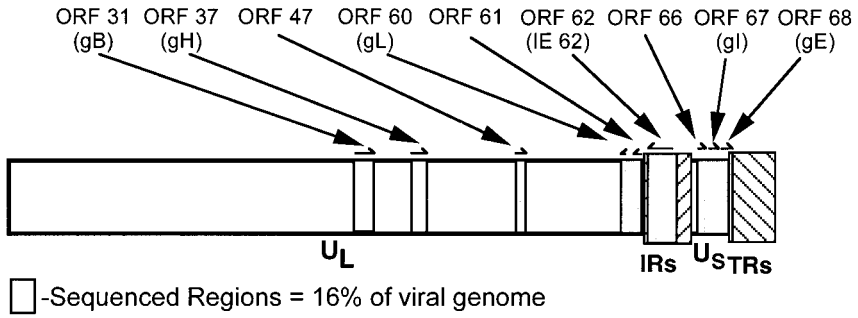

Nucleotides	Size of Region	ORF(s)	Substitutions
56767-57007	241	5' of ORF 31 (gB)	None
57008-59614	2607	ORF 31 (gB)	None
66074-68599	2526	ORF 37 (gH)	c66879t (P269L)
83168-84697	1530	ORF 47	None
101170-101649	480	ORF 60 (gL)	None
101650-103081	1432	5' of ORF 60 (gL)	a102203g a102575g c102617t a102969g
103082-104485	1404	ORF 61	None
104486-104936	450	5' of ORF 61	a104898g
105201-109133	3933	ORF 62 (IE62)	c109044g (A90A)
109134-109659	525	5' of ORF 62	None
113037-114218	1182	ORF 66	a114140g (S368S)
114219-114495	277	5' of ORF 67 (gI)	None
114496-115560	1065	ORF 67 (gI)	None
115561-115807	247	5' of ORF 68 (gE)	None
115808-117679	1872	ORF 68 (gE)	g116255a (D150N)

FIG. 7. Summary of genetic analysis of VZV-MSP. Each region of DNA was amplified from VZV-MSP and sequenced. Each DNA sequence was compared to the prototype VZV-Dumas sequence. All mutations discovered are listed by the nucleotide number of the Dumas strain. Any substitutions within open reading frames are followed by the predicted amino acid expressed by VZV-MSP. Accession numbers are listed in Materials and Methods.

sequences of VZV-Dumas. Further, the gB sequence was identical to that of VZV-Dumas. However, VZV-MSP gH contained a single point mutation within codon 269 (CCA → CTA), converting a proline residue in the predicted VZV-Dumas peptide sequence to a leucine residue in VZV-MSP gH.

Given the presence of mutations within VZV-MSP gE and gH, we performed similar genetic analyses of VZV-32. As expected, VZV-32 lacked the D150N mutation within gE. VZV-32 gH, however, revealed the identical point mutation found within codon 269 of VZV-MSP gH. Thus, the mutation within VZV-MSP gH cannot account for the VZV-MSP cell-spread phenotype. VZV-32 contained one additional mutation within ORF 67 (gI) which would lead to a Q5H substitution (CAA → CAT). This substitution was within the probable leader sequence of VZV gI and thus would not be present in mature gI (Davison and Scott, 1986). Altogether, within five major glycoprotein ORFs, VZV-MSP contained two point mutations which caused amino acid substitutions when compared to VZV-Dumas: D150N in gE and P269L in gH (Fig. 7).

In addition to five ORFs, we sequenced major portions of the 5′ untranslated regions of ORFs 31, 60, 67, and 68. All regions were identical to VZV-Dumas except for that of ORF 60. The latter region contained four polymorphisms; these ranged from 554 to 1320 nucleotides from the ORF 60 initiation codon (Fig. 7). It is very unlikely that these polymorphisms will alter the expression of gL since they are located over 500 nucleotides upstream of the gL start site.

Genetic analysis of VZV-MSP regulatory proteins and kinases

Although viral glycoproteins are the most likely candidates for mediating the cell-to-cell spread phenotype of VZV-MSP, we considered the possibility that an alteration in immediate early regulatory events may contribute to this enhanced cell-to-cell spread phenotype. VZV expresses one predominant species, IE 62, which acts as the major regulatory protein for viral gene expression (Perera *et al.,* 1992, 1993; Piette *et al.,* 1995; Shiraki and Hyman, 1987). This protein contains a potent acidic activation domain at its N-terminus and is a component of the virus particle (Kinchington *et al.,* 1992; Perera *et al.,* 1993). Therefore, we sequenced the IE 62 gene of VZV-MSP, but detected only one silent polymorphism within codon 30 when compared to the Dumas strain (GCG → GCC) (Fig. 7). Thus, the peptide sequence of VZV-MSP IE 62 was identical to the predicted VZV-Dumas sequence. Further, we sequenced the 5′ untranslated region containing 525 nucleotides and this region was identical to that of VZV-Dumas. In addition, we sequenced the adjacent VZV-MSP ORF 61, which encodes the functional homolog of HSV-1 ICP0 (Moriuchi *et al.,* 1992). Again, the nucleotide sequence was identical to that of VZV-Dumas.

Previous studies have shown that the viral protein kinase VZV ORF 47 can phosphorylate IE 62 (Ng, *et al.,* 1994). Also, VZV ORF 66 encodes a protein kinase which has been shown to affect the intracellular localization and transactivation function of IE 62 (Kinchington and Turse, 1998; Kinchington *et al.,* 2000). Based upon these results, we wanted to determine whether mutations in these viral kinases could affect the function of IE 62 within VZV-MSP-infected cells. Therefore, we sequenced both protein kinase genes within the VZV-MSP genome and found both to be identical to the prototype VZV-Dumas sequence (Fig. 7). Thus, there was no genetic evidence of polymorphisms within either of two regulatory ORFs or either of two viral protein kinase ORFs. In short, after sequence analysis of over 15% of the VZV-MSP genome, the main impression was a striking similarity with VZV-Dumas except for the notable exceptions mentioned earlier.

DISCUSSION

VZV-MSP represents the first reported antigenic variant of VZV gE or any other virion envelope protein. We have previously characterized the effect of the MSP mutation within gE (D150N) on the epitope of the anti-gE 3B3 antibody (Santos *et al.,* 1998). This amino acid substitution greatly reduces the affinity of MAb 3B3 to gE, causing loss of antibody recognition under normal conditions in both immunofluorescence and Western blot assays. We observed that this mutation was identical to a known amino acid substitution caused by antigenic drift in the influenza A hemagglutinin protein and postulated that VZV-MSP is an escape mutant that circumvents the antibody response following VZV infection (Szomolanyi-Tsuda and Welsh, 1998; Wharton *et al.,* 1989). We also have previously reported that VZV-MSP has a dramatically different topography of viral egress onto the surface of infected cultured cells compared to VZV-32 and VZV-Oka. The latter two strains normally emerge in a pattern which we have designated "viral highways" (Harson and Grose, 1995; also see cover photo of *Virology,* **249,** Sept. 15, 1998). However, VZV-MSP viral particles were more plentiful and more evenly distributed across the entire surface of infected cells in a pattern that was similar to the egress of HSV-1-infected cells (Padilla *et al.,* 1997; Santos *et al.,* 1998).

Taylor-Robinson and Caunt (1972) detailed the spread of VZV in cell culture in 1972. They noted that small foci ("microplaques") were first detected at 2 days postinfection; the foci subsequently enlarged over the next 4–8 days. When Cohen and Straus (1996) reviewed the topic of VZV growth in cultured cells 24 years later, studies during the intervening decades had revealed relatively little new information about viral variants. One problem with assessing differences between strains in VZV spread and infectivity is the cell-associated nature of VZV infection in cultured cells. Numerous investigations over several decades have discovered that attempts to quantitate cell-free virus invariably lead to simultaneous loss of infectivity, possibly due to loss of the viral envelope. Thus, most studies are performed with an inoculum of infected cells rather than cell-free virus.

To circumvent difficulties with virus titration by more traditional assays, we adapted a software program called Brainvox tal_support systems to analyze confocal images of VZV-infected monolayers (Frank *et al.,* 1997). In confocal microscopic analysis, a laser scans the sample line by line, generating an excitation signal as it passes over fluorophores coupled to the secondary antibody. After this excitation signal enters the photomultiplier tube, each pixel of the digital image is assigned an intensity determined by the amount of fluorescence of that site in the original sample. The range of the gray scale is from 0 to 255 (8 bit). The software program calculated for each VZV confocal image the intensity of the fluorescent signal within each pixel. In general, the background as determined with uninfected cell controls had a pixel intensity of less than 25, while positive cells had a pixel intensity within the 25–255 range. Thereafter, the Brainvox tal_support programs were instructed to extract the positive pixels and plot the data as a histogram representing VZV IE-62-positive cells. Through this quantitative imaging approach, we were able to document an accelerated cell-to-cell spread phenotype of VZV-MSP.

After we had documented two distinct components of the VZV-MSP phenotype (pattern of viral egress and enhanced cell-to-cell spread), we postulated that VZV-MSP would behave differently in the SCID-hu mouse model. VZV has a highly restricted host range and previous attempts to study the virus in a variety of experimental animals did not mimic the symptomatic disease in humans (Arvin, 1996). By implanting human fetal skin tissue into SCID-hu mice, an animal model was established which allowed VZV replication in differentiated human skin with subsequent formation of vesicular lesions, the hallmark of human clinical disease (Moffat *et al.,* 1995). These studies documented a correlation between (i) high infectious foci counts, (ii) increased histopathology, and (iii) detectable enveloped virions in the implants (Moffat *et al.,* 1998a). The morphological features of virions from skin implants closely resemble the complete enveloped virions seen in samples collected from human vesicular fluid; in contrast, samples collected from infected cell cultures rarely show a prototypic enveloped virion but exhibit a spectrum of aberrant particles (Grose *et al.,* 1995). In the prior study, enveloped virions were detected in the skin implants 21 days postinfection with wild-type virus but not vaccine Oka virus (Moffat *et al.,* 1998a). The fact that virus was detected in VZV-MSP-infected implants at 14 days postin-

fection in the current study reinforces the correlation recognized in the 1998 study.

Previous studies in SCID-hu mice have demonstrated a reduced virulence of the vaccine strain of VZV-Oka in comparison to the parental VZV-Oka strain (Moffat *et al.,* 1998a). The pathogenic properties of laboratory generated VZV mutants have also been assessed. In one example, a VZV-ORF 47 deletion mutant replicated efficiently in cultured cells *in vitro* but could not replicate within differentiated human cells in the SCID-hu model, a result which highlighted the importance of this viral kinase *in vivo* (Moffat *et al.,* 1998b). Thus, the SCID-hu model has facilitated the characterization of VZV strains with reduced virulence in differentiated lymphocytes and skin cells. In juxtaposition, we have now documented for the first time in the SCID-hu animal model an accelerated pathogenesis of VZV-MSP over that of other VZV wild-type isolates and laboratory strains.

The phenotype of the VZV gE mutant virus led us to reexamine the data about the role of this glycoprotein in cell-to-cell spread. VZV gE is a 623-amino-acid, type I transmembrane glycoprotein (Davison and Scott, 1986). Within the VZV system, gE is considered to be an essential glycoprotein (Mallory *et al.,* 1997). VZV gE forms a heterodimer with gI, a 354-amino-acid, type I transmembrane glycoprotein whose cytoplasmic tail also contains both endocytosis and phosphorylation motifs (Olson *et al.,* 1997; Olson and Grose, 1998; Zhu *et al.,* 1996). The gE and gI glycoproteins interact via their ectodomains (Kimura *et al.,* 1997). Not only is VZV gI required for replication of the virus in Vero cells, but also VZV gI deletion mutants in melanoma cells show a reduced cell-to-cell spread phenotype, highlighting the role of this protein in cell-to-cell spread (Cohen and Nguyen, 1997; Cohen and Seidel, 1993; Mallory *et al.,* 1997). In addition, VZV gI acts as a chaperone protein and can facilitate the efficient endocytosis and subcellular trafficking of gE lacking its endocytosis motif (Olson and Grose, 1998). Of interest, gE cannot perform the same function for a disabled gI protein.

The role of gE in mediating cell-to-cell spread has been well studied in both HSV-1 and PRV (Dingwell *et al.,* 1994, 1995; Dingwell and Johnson, 1998; Tirabassi *et al.,* 1997; Wisner *et al.,* 2000; Zsak *et al.,* 1992). Deletional mutants of HSV-1 gE and gI exhibit a reduced plaque size phenotype in tissue culture as well as reduced neuronal spread in a rat eye model (Dingwell *et al.,* 1994; Dingwell and Johnson, 1998). Studies in the PRV system with gE deletional mutants demonstrated a similar reduced spread in tissue culture and a rat eye model (Tirabassi *et al.,* 1997; Zsak *et al.,* 1992). However, HSV-1 gE mutants which still expressed the gE ectodomain yet lacked the cytoplasmic domain failed to restore cell-to-cell spread in tissue culture, but the ectodomain was able to mediate localization of gE to tight junctions between cells (Wisner *et al.,* 2000). In contrast, similar PRV gE truncation mutants which still expressed the gE ectodomain showed partial restoration of cell-to-cell spread in tissue culture as well as neurotropic spread in the rat visual system similar to wild-type virus (Tirabassi *et al.,* 1997). Thus, in studies of alphaherpesviruses other than VZV, gE plays a crucial role in cell-to-cell spread, and the gE ectodomain alone can mediate some of these functions.

We have now sequenced ~20 kb of the VZV-MSP genome, including the ORFs of five glycoproteins, two major VZV regulatory proteins, two viral kinases, and major portions of the 5′ untranslated regions of these ORFs. After evaluating these sequence data, we were struck by the overall identity of VZV-MSP to the prototype VZV-Dumas. Although a few polymorphisms were noted, the majority of these were in untranslated regions (Fig. 7). Other than the previously reported change within VZV-MSP gE, only one polymorphism (within VZV-MSP gH) led to a predicted amino acid substitution. Within the VZV system the gH:gL complex subsumes a prominent role in fusion (Duus *et al.,* 1995; Rodriguez *et al.,* 1993). In contrast to HSV-1, monolayers transfected with only the VZV gH and VZV gL genes are completely fused (Duus *et al.,* 1995; Duus and Grose, 1996; Turner *et al.,* 1998). Yet, it appeared unlikely that the one-point mutation at position 269 within gH contributed to the VZV-MSP phenotype because the same mutation was found in gH of the laboratory strain VZV-32. In summary, the above data have strengthened the original observation that the variant virus has a phenotype clearly distinguishable from any VZV strain previously studied by the authors of this article.

MATERIALS AND METHODS

Cells, viruses, and transfer of infectivity

VZV-MSP was isolated in Minnesota in late 1995 (Santos *et al.,* 1998). VZV-32 was isolated in Texas in the 1970s (Grose and Brunell, 1978). Reserve stocks of VZV-32 and VZV-MSP were prepared; thus low passages (<20) were used in all experiments in this report. VZV-Oka was isolated in Japan and attenuated in the 1970s (Takahashi *et al.,* 1975). VZV-Dumas was isolated in Holland and sequenced in its entirety by Davison and Scott (1986). All strains were propagated in human melanoma cells (MeWo strain). MeWo cells are highly permissive for VZV replication with no release of infectious virus into the culture medium (Grose, 1980). Transfer of infectivity was carried out by inoculation of trypsin-dispersed infected cells onto an uninfected monolayer at a 1:8 ratio of infected:uninfected cells unless otherwise noted (Grose and Brunell, 1978). Similarly, infectious center assays were carried out by described methods; these assays included both melanoma cell and human neonatal foreskin cell substrates (Cole and Kingsley, 1992; Grose and Brunell, 1978).

Imaging by confocal microscopy

Replicate 35-mm monolayers of MeWo cells were overlaid with VZV-infected cells at a 1:8 ratio of infected: uninfected cells. At 4, 8, 12, 24, and 48 h postinfection, the monolayers were fixed and permeabilized with 0.5 ml of 2% paraformaldehyde with 0.05% Triton X-100. Cells were probed with an anti-IE-62 mouse monoclonal ascites (MAb 5C6) at a dilution of 1:1000 (Ng *et al.,* 1994). The secondary antibody was goat anti-mouse IgG $F(ab')_2$ conjugated to Alexa 488 at a dilution of 1:2500 (Molecular Probes). Cell nuclei were stained with TOTO-3 (Molecular Probes), a dimeric cyanine nucleic acid stain, at a dilution of 1:10,000. Samples were examined with a Bio-Rad 1024 laser scanning confocal microscope, as described (Duus *et al.,* 1995).

Quantitative analysis of confocal images

Confocal images were converted to TIFF format images (Confocal Assistant, v. 4.02) and transferred to a Silicon Graphics Indy workstation in order to produce the color prints by Showcase software program. Confocal images also were analyzed with the Brainvox tal_support programs (Frank *et al.,* 1997). Similar analyses can be performed with the public domain NIH Image program, which was developed at the U.S. National Institutes of Health (http://rsb.info.nih.gov/nih-image/).

Replication in the SCID-hu mouse

The SCID-hu mouse has been established as an animal model for VZV replication (Moffat *et al.,* 1995). In this model, C.B-17 *scid/scid* mice were implanted with fetal skin tissue subcutaneously as full-thickness dermal grafts. Human fetal tissues were obtained with informed consent according to federal and state regulations and were screened for human immunodeficiency virus. The general care of the experimental animals used for this study was in accordance with the National Institutes of Health guidelines for laboratory animals and in compliance with the Animal Welfare Act (Public Law 94-279) as well as the Stanford University Administrative Panel on Laboratory Animal Care. Animal inoculations were performed according to the previously described protocol (Moffat *et al.,* 1995), viz., an aliquot of infected cell suspension containing 10^5 infectious centers was injected into each implant. Mock-infected implants were injected with human cells alone. Skin implants were harvested at 7, 14, and 21 days postinoculation. The implants were fixed in 4% paraformaldehyde, paraffin-embedded, cut into 3-μm sections, and stained with hematoxylin and eosin. Tissue sections were examined on a Leitz Diaplan light microscope, and digital images were acquired with an Optronics DEI 750 digital camera (Optronics Engineering). Digital images were formatted as described above.

Isolation of viral DNA

For all viral strains, a 25-cm^2 monolayer of MeWo cells was infected as described above. After development of 80–100% cytopathology, the infected monolayer was washed thrice with 0.5 ml of 0.01 M phosphate-buffered saline (PBS), pH 7.4. Infected cells were then harvested by dislodging into 0.5 ml of PBS. Viral DNA was collected with a DNAeasy kit following the Blood and Body Fluid Protocol (Qiagen, Inc.). Following the DNAeasy protocol, DNA was placed onto a Microcon 50 filter (Millipore) and washed twice with 0.5 ml of Nanopure water (Barnstead/Thermolyne). Viral DNA was resuspended in 100 μL of Nanopure water. DNA concentration was assessed visually after 1% agarose gel electrophoresis.

PCR amplification and sequencing of VZV genes

For each ORF, a pair of flanking primers was designed to amplify the gene of interest. PCR amplifications were performed with the Expand High-Fidelity PCR system (Boehringer Mannheim). This system utilizes both Taq DNA and Pwo DNA polymerases, with the 3′–5′ proofreading activity of Pwo DNA polymerase allowing increased fidelity (8.5×10^{-6}/bp error rate) (Boehringer Mannheim). After amplification, the PCR product was sequenced by using the dye terminator cycle sequencing chemistry with AmpliTaq DNA polymerase, FS enzyme (Perkin–Elmer Applied Biosystems, Foster City, CA). Sequencing reactions were performed on and analyzed with an Applied Biosystems Model 373A stretch fluorescent automated sequencer (Perkin–Elmer) at the University of Iowa DNA facility. All genes were PCR amplified twice and each PCR fragment was sequenced at least twice to confirm reported mutations. The accession number for the complete VZV-Dumas sequence is X04370.

GenBank deposition

The genomic sequences of VZV-MSP described in the Results were submitted to GenBank, Bethesda, Maryland. The accession numbers for the six viral DNA segments are AY005330, AY005331, AY005332, AY005333, AY005334 and AY005335.

ACKNOWLEDGMENTS

This research was supported by NIH Grants AI36884, AI22795, AI20459, F31-DC00201, and HD07249 and a grant from the VZV Research Foundation. Imaging studies were performed at the University of Iowa Central Microscopy Research Facility. We thank Boyd Knosp at the Iowa Image Analysis Facility for his technical assistance.

REFERENCES

Arvin, A. M. (1996). Varicella-zoster virus. *In* "Virology" (B. N. Fields, D. N. Knipe, and P. M. Howley, Eds.), pp. 2547–2585. Lippincott–Raven, Philadelphia.

Arvin, A. M., Kinney-Thomas, E., Shriver, K., Grose, C., Koropchak, C. M., Scranton, E., Wittek, A. E., and Diaz, P. S. (1986). Immunity to varicella-

zoster viral glycoproteins, gp I (gp 90/58) and gp III (gp 118), and to a nonglycosylated protein, p 170. *J. Immunol.* **137,** 1346–1351.

Bergen, R. E., Sharp, M., Sanchez, A., Judd, A. K., and Arvin, A. M. (1991). Human T cells recognize multiple epitopes of an immediate early/tegument protein (IE62) and glycoprotein I of varicella zoster virus. *Viral Immunol.* **4,** 151–166.

Cohen, J. I., and Nguyen, H. (1997). Varicella-zoster virus glycoprotein I is essential for growth of virus in Vero cells. *J. Virol.* **71,** 6913–6920.

Cohen, J. I., and Seidel, K. E. (1993). Generation of varicella-zoster virus (VZV) and viral mutants from cosmid DNAs: VZV thymidylate synthetase is not essential for replication in vitro. *Proc. Natl. Acad. Sci. USA* **90,** 7376–7380.

Cohen, J. I., and Straus, S. E. (1996). Varicella-zoster virus and its replication. *In* "Virology" (B. N. Fields, D. N. Knipe, and P. M. Howley, Eds.), pp. 2525–2545. Lippincott–Raven, Philadelphia.

Cole, N. L., and Kingsley, R. E. (1992). Colchicine treatment in the preparation of varicella-zoster virus inocula. *J. Virol. Methods* **36,** 111–118.

Davison, A. J., and Scott, J. E. (1983). Molecular cloning of the varicella-zoster virus genome and derivation of six restriction endonuclease maps. *J. Gen. Virol.* **64,** 1811–1814.

Davison, A. J., and Scott, J. E. (1986). The complete DNA sequence of varicella-zoster virus. *J. Gen. Virol.* **67,** 1759–1816.

Dingwell, K. S., Brunetti, C. R., Hendricks, R. L., Tang, Q., Tang, M., Rainbow, A. J., and Johnson, D. C. (1994). Herpes simplex virus glycoproteins E and I facilitate cell-to-cell spread in vivo and across junctions of cultured cells. *J. Virol.* **68,** 834–845.

Dingwell, K. S., Doering, L. C., and Johnson, D. C. (1995). Glycoproteins E and I facilitate neuron-to-neuron spread of herpes simplex virus. *J. Virol.* **69,** 7087–7098.

Dingwell, K. S., and Johnson, D. C. (1998). The herpes simplex virus gE–gI complex facilitates cell-to-cell spread and binds to components of cell junctions. *J. Virol.* **72,** 8933–8942.

Duus, K. M., and Grose, C. (1996). Multiple regulatory effects of varicella-zoster virus (VZV) gL on trafficking patterns and fusogenic properties of VZV gH. *J. Virol.* **70,** 8961–8971.

Duus, K. M., Hatfield, C., and Grose, C. (1995). Cell surface expression and fusion by the varicella-zoster virus gH:gL glycoprotein complex: Analysis by laser scanning confocal microscopy. *Virology* **210,** 429–440.

Frank, R. J., Damasio, H., and Grabowski, T. J. (1997). Brainvox: An interactive, multimodal visualization and analysis system for neuroanatomical imaging. *Neuroimage* **5,** 13–30.

Grose, C. (1980). The synthesis of glycoproteins in human melanoma cells infected with varicella-zoster virus. *Virology* **101,** 1–9.

Grose, C. (1990). Glycoproteins encoded by varicella-zoster virus: Biosynthesis, phosphorylation, and intracellular trafficking. *Annu. Rev. Microbiol.* **44,** 59–80.

Grose, C. (1999). Varicella-zoster virus: less immutable than once thought. *Pediatrics* **103,** 1027–1028.

Grose, C., and Brunell, P. A. (1978). Varicella-zoster virus: isolation and propagation in human melanoma cells at 36 and 32 degrees C. *Infect. Immun.* **19,** 199–203.

Grose, C., Harson, R., and Beck, S. (1995). Computer modeling of prototypic and aberrant nucleocapsids of varicella-zoster virus. *Virology* **214,** 321–329.

Harson, R., and Grose, C. (1995). Egress of varicella-zoster virus from the melanoma cell: a tropism for the melanocyte. *J. Virol.* **69,** 4994–5010.

Ito, M., Ihara, T., Grose, C., and Starr, S. (1985). Human leukocytes kill varicella-zoster virus-infected fibroblasts in the presence of murine monoclonal antibodies to virus-specific glycoproteins. *J. Virol.* **54,** 98–103.

Kimura, H., Straus, S. E., and Williams, R. K. (1997). Varicella-zoster virus glycoproteins E and I expressed in insect cells form a heterodimer that requires the N-terminal domain of glycoprotein I. *Virology* **233,** 382–391.

Kinchington, P. R., Fite, K., and Turse, S. E. (2000). Nuclear accumulation of IE62, the varicella-zoster virus (VZV) major transcriptional regulatory protein, is inhibited by phosphorylation mediated by the VZV open reading frame 66 protein kinase. *J. Virol.* **74,** 2265–2277.

Kinchington, P. R., Hougland, J. K., Arvin, A. M., Ruyechan, W. T., and Hay, J. (1992). The varicella-zoster virus immediate-early protein IE62 is a major component of virus particles. *J. Virol.* **66,** 359–366.

Kinchington, P. R., and Turse, S. E. (1998). Regulated nuclear localization of the varicella-zoster virus major regulatory protein, IE62. *J. Infect. Dis.* **178**(Suppl. 1), S16–S21.

Litwin, V., Jackson, W., and Grose, C. (1992). Receptor properties of two varicella-zoster virus glycoproteins, gpI and gpIV, homologous to herpes simplex virus gE and gI. *J. Virol.* **66,** 3643–3651.

Litwin, V., Sandor, M., and Grose, C. (1990). Cell surface expression of the varicella-zoster virus glycoproteins and Fc receptor. *Virology* **178,** 263–272.

Mallory, S., Sommer, M., and Arvin, A. M. (1997). Mutational analysis of the role of glycoprotein I in varicella-zoster virus replication and its effects on glycoprotein E conformation and trafficking. *J. Virol.* **71,** 8279–8288.

McGeoch, D. J., and Cook, S. (1994). Molecular phylogeny of the alphaherpesvirinae subfamily and a proposed evolutionary timescale. *J. Mol. Biol.* **238,** 9–22.

McGeoch, D. J., Cook, S., Dolan, A., Jamieson, F. E., and Telford, E. A. (1995). Molecular phylogeny and evolutionary timescale for the family of mammalian herpesviruses. *J. Mol. Biol.* **247,** 443–458.

McGeoch, D. J., and Davison, A. J. (1999). The molecular evolutionary history of the herpesviruses. *In* "Origin and Evolution of Viruses" (E. Domingo, R. Webster, and J. Holland, Eds.), pp. 441–465. Academic Press, London.

Mo, C., Suen, J., Sommer, M., and Arvin, A. M. (1999). Characterization of varicella-zoster virus glycoprotein K (open reading frame 5) and its role in virus growth. *J. Virol.* **73,** 4197–4207.

Moffat, J. F., Stein, M. D., Kaneshima, H., and Arvin, A. M. (1995). Tropism of varicella-zoster virus for human CD4+ and CD8+ T lymphocytes and epidermal cells in SCID-hu mice. *J. Virol.* **69,** 5236–5242.

Moffat, J. F., Zerboni, L., Kinchington, P. R., Grose, C., Kaneshima, H., and Arvin, A. M. (1998a). Attenuation of the vaccine Oka strain of varicella-zoster virus and role of glycoprotein C in alphaherpesvirus virulence demonstrated in the SCID-hu mouse. *J. Virol.* **72,** 965–974.

Moffat, J. F., Zerboni, L., Sommer, M. H., Heineman, T. C., Cohen, J. I., Kaneshima, H., and Arvin, A. M. (1998b). The ORF47 and ORF66 putative protein kinases of varicella-zoster virus determine tropism for human T cells and skin in the SCID-hu mouse. *Proc. Natl. Acad. Sci. USA* **95,** 11969–11974.

Moriuchi, H., Moriuchi, M., Smith, H. A., Straus, S. E., and Cohen, J. I. (1992). Varicella-zoster virus open reading frame 61 protein is functionally homologous to herpes simplex virus type 1 ICP0. *J. Virol.* **66,** 7303–7308.

Ng, T. I., Keenan, L., Kinchington, P. R., and Grose, C. (1994). Phosphorylation of varicella-zoster virus open reading frame (ORF) 62 regulatory product by viral ORF 47-associated protein kinase. *J. Virol.* **68,** 1350–1359.

Olson, J. K., Bishop, G. A., and Grose, C. (1997). Varicella-zoster virus Fc receptor gE glycoprotein: Serine/threonine and tyrosine phosphorylation of monomeric and dimeric forms. *J. Virol.* **71,** 110–119.

Olson, J. K., and Grose, C. (1997). Endocytosis and recycling of varicella-zoster virus Fc receptor glycoprotein gE: Internalization mediated by a YXXL motif in the cytoplasmic tail. *J. Virol.* **71,** 4042–4054.

Olson, J. K., and Grose, C. (1998). Complex formation facilitates endocytosis of the varicella-zoster virus gE:gI Fc receptor. *J. Virol.* **72,** 1542–1551.

Padilla, J. A., Uno, F., Yamada, M., Namba, H., and Nii, S. (1997). High-resolution immuno-scanning electron microscopy using a non-coating method: Study of herpes simplex virus glycoproteins on the surface of virus particles and infected cells. *J. Electron Microsc. (Tokyo)* **46,** 171–180.

Perera, L. P., Mosca, J. D., Ruyechan, W. T., Hayward, G. S., Straus, S. E., and Hay, J. (1993). A major transactivator of varicella-zoster virus, the immediate-early protein IE62, contains a potent N-terminal activation domain. *J. Virol.* **67,** 4474–4483.

Perera, L. P., Mosca, J. D., Sadeghi-Zadeh, M., Ruyechan, W. T., and Hay, J. (1992). The varicella-zoster virus immediate early protein, IE62, can positively regulate its cognate promoter. *Virology* **191,** 346–354.

Piette, J., Defechereux, P., Baudoux, L., Debrus, S., Merville, M. P., and Rentier, B. (1995). Varicella-zoster virus gene regulation. *Neurology* **45,** S23–S27.

Rodriguez, J. E., Moninger, T., and Grose, C. (1993). Entry and egress of varicella virus blocked by same anti-gH monoclonal antibody. *Virology* **196,** 840–844.

Santos, R. A., Padilla, J. A., Hatfield, C., and Grose, C. (1998). Antigenic variation of varicella zoster virus Fc receptor gE: Loss of a major B cell epitope in the ectodomain. *Virology* **249,** 21–31.

Shiraki, K., and Hyman, R. W. (1987). The immediate early proteins of varicella-zoster virus. *Virology* **156,** 423–426.

Szomolanyi-Tsuda, E., and Welsh, R. M. (1998). T-cell-independent antiviral antibody responses. *Curr. Opin. Immunol.* **10,** 431–435.

Takahashi, M., Okuno, Y., Otsuka, T., Osame, J., and Takamizawa, A. (1975). Development of a live attenuated varicella vaccine. *Biken J.* **18,** 25–33.

Taylor-Robinson, D., and Caunt, A. E. (1972). Varicella virus. *Virol. Monogr.* **12,** 1–88.

Tirabassi, R. S., and Enquist, L. W. (1999). Mutation of the YXXL endocytosis motif in the cytoplasmic tail of pseudorabies virus gE. *J. Virol.* **73,** 2717–2728.

Tirabassi, R. S., Townley, R. A., Eldridge, M. G., and Enquist, L. W. (1997). Characterization of pseudorabies virus mutants expressing carboxy-terminal truncations of gE: Evidence for envelope incorporation, virulence, and neurotropism domains. *J. Virol.* **71,** 6455–6464.

Turner, A., Bruun, B., Minson, T., and Browne, H. (1998). Glycoproteins gB, gD, and gHgL of herpes simplex virus type 1 are necessary and sufficient to mediate membrane fusion in a Cos cell transfection system. *J. Virol.* **72,** 873–875.

Weller, T. H. (1953). Serial propagation in vitro of agents producing inclusion bodies derived from varicella and herpes zoster. *Proc. Soc. Exp. Biol. Med.* **83,** 340–346.

Wharton, S. A., Weis, W., Skehel, J. J., and Wiley, D. C. (1989). Structure, function and antigenicity of the hemagglutinin of influenza viruses. *In* "The Influenza Viruses" (R. M. Krug, Ed.), pp. 153–169. Plenum Press, New York.

Wisner, T., Brunetti, C., Dingwell, K., and Johnson, D. C. (2000). The extracellular domain of herpes simplex virus gE is sufficient for accumulation at cell junctions but not for cell-to-cell spread. *J. Virol.* **74,** 2278–2287.

Yamanishi, K., Matsunaga, Y., Ogino, T., Takahashi, M., and Takamizawa, A. (1980). Virus replication and localization of varicella-zoster virus antigens in human embryonic fibroblast cells infected with cell-free virus. *Infect. Immun.* **28,** 536–541.

Yao, Z., Jackson, W., and Grose, C. (1993). Identification of the phosphorylation sequence in the cytoplasmic tail of the varicella-zoster virus Fc receptor glycoprotein gpI. *J. Virol.* **67,** 4464–4473.

Ye, M., Duus, K. M., Peng, J., Price, D. H., and Grose, C. (1999). Varicella-zoster virus Fc receptor component gI is phosphorylated on its endodomain by a cyclin-dependent kinase. *J. Virol.* **73,** 1320–1330.

Zhu, Z., Hao, Y., Gershon, M. D., Ambron, R. T., and Gershon, A. A. (1996). Targeting of glycoprotein I (gE) of varicella-zoster virus to the trans-Golgi network by an AYRV sequence and an acidic amino acid-rich patch in the cytosolic domain of the molecule. *J. Virol.* **70,** 6563–6575.

Zsak, L., Zuckermann, F., Sugg, N., and Ben-Porat, T. (1992). Glycoprotein gI of pseudorabies virus promotes cell fusion and virus spread via direct cell-to-cell transmission. *J. Virol.* **66,** 2316–2325.